International Journal of Engineering and Technology Innovation, vol. 16, no. 2, 2026, pp. 179-198

Dynamic Response and Shear Mechanisms of Reinforced Concrete Columns Subjected to Lateral Impact

Zhihan Hou[1], Jiawen Xu[2], Jingming Sun[3,*], Fei Luo[2], Wangqiang Zhao[2]

[1] The Institute of Shanxi Architectural Design And Research Co., Ltd., Taiyuan, China

[2] Shanxi Academy of Building Sciences Group Co., Ltd., Taiyuan, China

[3] School of Civil Engineering and Architecture, Linyi University, Linyi, China

Received 21 October 2025; received in revised form 02 February 2026; accepted 04 February 2026

DOI: https://doi.org/10.46604/ijeti.2026.15815

Abstract

This study investigates the dynamic response and shear failure mechanisms of reinforced concrete (RC) columns under lateral impacts, such as vehicle collisions. A three-dimensional nonlinear finite element (FE) model is developed, incorporating concrete damage, reinforcement plasticity, and strain-rate effects. The numerical model is validated against experimental pendulum impact tests. Parametric analyses are conducted to evaluate the effects of impact severity, axial compression ratio, stirrup ratio, longitudinal reinforcement ratio, slenderness ratio, and concrete strength on failure modes. Results indicate that impact-induced diagonal cracking governs the transition from non-failure to punching-shear failure. Increasing the stirrup ratio and concrete strength delays brittle shear failure, whereas excessive axial compression promotes shear localization. The findings provide insights into the impact-resistant behavior of RC columns and offer guidance for improving structural design against lateral impact loads.

Keywords: lateral impact, shear mechanism, reinforced concrete column, finite element simulation, parametric analysis

1. Introduction

Reinforced concrete (RC) columns are essential structural components that support vertical loads in buildings and infrastructure. They are widely used in structures such as high-rise buildings and bridges. During their service life, RC columns are subjected not only to long-term static loads but also to sudden extreme events, such as earthquakes [1-2], vehicle collisions [3-4], and explosions [5-6]. These events elicit dynamic responses that are significantly distinct from static behavior. RC columns in highway bridges, port terminals, and other typical engineering applications are especially susceptible to inadvertent collisions with large vessels or overweight vehicles. These unexpected lateral impacts generally involve substantial masses at relatively low velocities and may cause severe localised damage or even total structural failure. Therefore, understanding the dynamic response and failure mechanisms of RC columns under lateral impact is essential for impact-resistant design and public safety.

A substantial body of experimental and numerical research, both domestically and internationally, has assessed the impact resistance and failure mechanisms of RC columns subjected to collision-type loading (e.g., vehicle impacts). These studies indicate that vertical members, such as bridge piers, may incur significant damage or even fail during collisions, highlighting the necessity of considering impact loads in design [7-8]. El-Tawil et al. [9] observed in bridge-pier collision tests that vehicle impacts can significantly diminish load-bearing and potentially lead to catastrophic failure. Consequently, bridge design codes

* Corresponding author. E-mail address: gzdxyjssjm@163.com

such as the AASHTO LRFD Bridge Design Specifications prescribe minimum impact resistance requirements for bridge piers to ensure structural safety. Nevertheless, structural responses under impact are highly nonlinear and strain-rate dependent. Elevated strain rates can increase material strength, facilitate stress-wave propagation, and provoke localized failure behaviors that significantly from those observed under static loading [10].

Comprehensive investigations have shown that RC columns subjected to impact loads often exhibit failure modes that differ from those observed under static conditions, with brittle shear failure being more pronounced. The stirrup ratio and impact velocity significantly affect the failure patterns. Existing studies consistently indicate that the stirrup ratio governs the impact-induced failure mode: insufficient transverse reinforcement promotes brittle diagonal shear failure, whereas increasing stirrup ratios delays shear cracking and shifts the failure mode towards flexural or flexure–shear behavior [8, 11-13].

Impact velocity also influences crack development. At low velocities, flexural cracks generally commence at the column base and propagate upward, resulting in flexure-dominated deformation . In contrast, at higher velocities, diagonal cracks may first initiate in the impact region and extend downward, leading to shear-dominated failure characteristics. These observations indicate that the load-bearing mechanisms of RC columns under impact differ significantly from those under static conditions, with shear failure frequently emerging as the predominant mode. Further research is therefore needed to clarify the initiation and evolution of impact-induced shear failure mechanisms in RC columns.

The impact resistance of RC columns is contingent upon various parameters. In addition to the size and energy of the impact, structural parameters and boundary conditions significantly influence the dynamic response,. Research indicates that, within a certain range, increasing the axial compression ratio can enhance impact resistance; however, excessive axial compression aggravates structural damage and shifts the failure mode from ductile flexural to brittle shear [12, 14]. Higher impact velocities markedly enhance structural damage: both the peak impact force and column deformation rise with velocity, resulting in a transition from flexural to shear-dominated failure [12].

Furthermore, varying combinations of impact mass and velocity—despite having identical total impact energy—elicit divergent responses. A large mass at low velocity yields a long-duration impact and larger global displacement dominated by flexural deformation, whereas a small mass at high velocity produces a short-duration impact that tends to cause localized shear damage. Collision tests on axially loaded circular RC columns have shown that increasing axial compression ratio and impact velocity can shift the failure mode from flexural to shear, markedly diminishing residual load-carrying capacity [15]. Numerical studies further indicate that parameters such as the axial compression ratio significantly influence the failure mode and the severity of damage [16]. Additional factors, including the stirrup ratio, longitudinal reinforcement ratio, and slenderness ratio, also affect the distribution of impact forces and energy dissipation in the columns [17-19].

To address these gaps, this study develops a validated finite element (FE) model to investigate the shear failure process of RC columns subjected to lateral impact. The model is validated against published experimental results [11]. Compared with recent closely related studies (including Sun et al. and others), which mainly report global response indicators or consider limited parameter variations, this study emphasizes a mechanism-oriented interpretation. It contributes new insights in three aspects: (i) it clarifies the evolution of impact-induced diagonal cracking and the development of shear-governed failure in relation to inertia effects and strain-rate-dependent material behavior; (ii) it provides a systematic, multi-parameter assessment of failure-mode transitions trends under variations in axial compression ratio, stirrup ratio, slenderness ratio, reinforcement ratio, impact mass–velocity combinations, and concrete strength; and (iii) it explicitly discusses the interaction between shear force and bending moment under impact loading, offering a clearer basis for interpreting shear-dominant versus flexure-dominant responses. The findings provide mechanistic insight and technical references for impact-resistant design of RC columns.

2. Finite Element Modelling and Validation

This section describes the experimental setup used to investigate the dynamic response of RC columns under lateral impact. The key focus is on describing the materials, reinforcement details, and the testing apparatus used in the pendulum impact tests. The measured quantities, such as impact force histories, displacement responses, and observed damage patterns, are presented to provide a benchmark for validating the FE model developed in this study.

2.1. Experimental program and measurements

Sun et al. [11] performed pendulum impact tests to investigate the dynamic response of RC columns under varying axial compression ratios. In these experiments, the longitudinal reinforcement had a diameter of 18 mm with a yield strength of 482 MPa, whereas the stirrups were 6 mm in diameter with a yield strength of 421 MPa. The mean compressive strength of the concrete was 29 MPa. The experimental configuration included an axial loading system, a support framework, and a pendulum impact mechanism, as illustrated in Fig. 1(a).

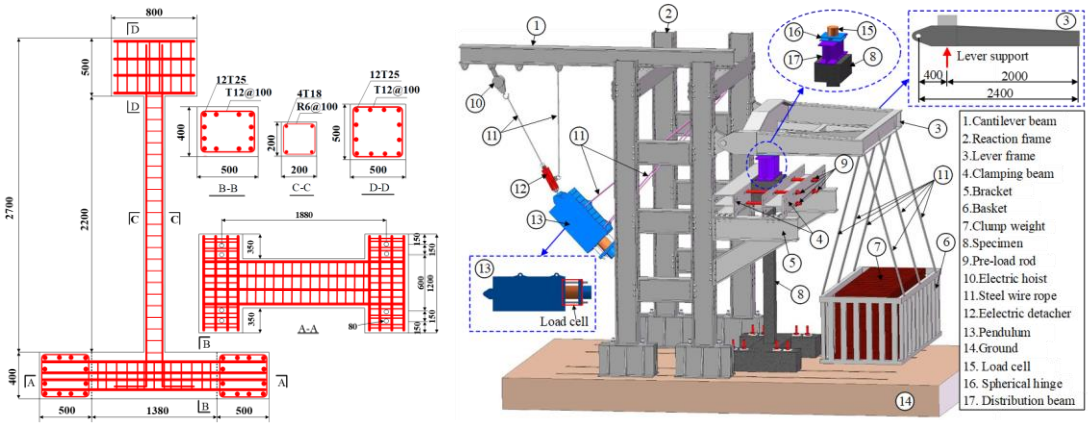

(a) Specimen dimensions and reinforcement details [11]

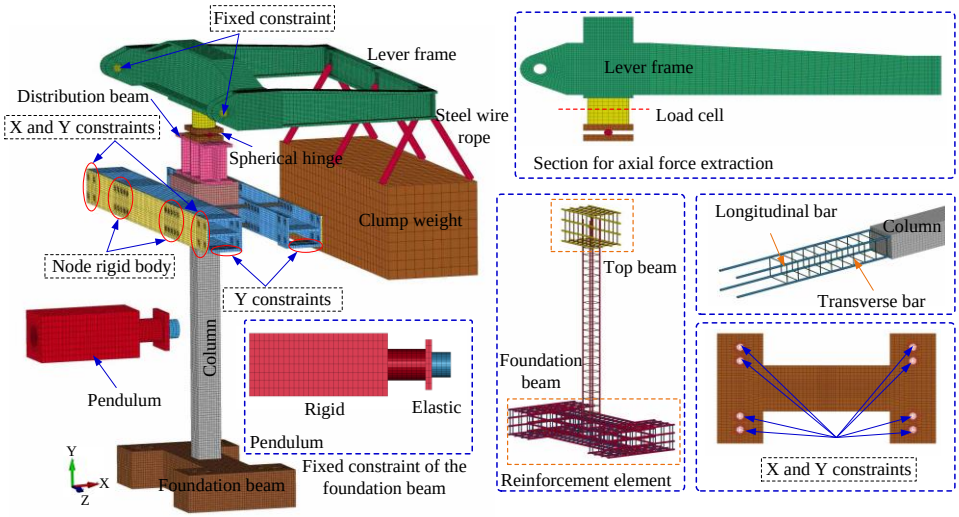

(b) Numerical analysis model

Fig. 1 Pendulum impact test and mode

The column cap was restrained by a steel reaction frame, allowing onely axial deformation. At the same time, the base was connected to the foundation with eight anchor bolts to ensure stable boundary conditions. The pendulum impact apparatus comprised an electric release device, an electric hoist, a steel wire rope, a pendulum, and the test specimen. The hammerhead had a cylindrical body 200 mm in diameter. To enhance end-restraint stiffness, the column cap and base were cast monolithically with the concrete.

Test measurements and data acquisition. During the pendulum impact tests, the primary recorded responses included: (1) the impact force–time history, measured using the force sensor integrated in the impact system; (2) the lateral displacement–time history at the impact location(mid-height), obtained from displacement transducers; and (3) the axial load level, monitored throughout the test to maintain the target axial compression condition. In addition, damage evolution and final crack patterns were documented through visual inspection and photographic records after each test. These measured quantities (impact force, lateral displacement, and damage morphology) are subsequently used as benchmark data for the FE model validation presented in Section 2.3.

2.2. Finite element model development

In the finite-element modelling, all components are depicted as full-scale three-dimensional models at a 1:1 scale. Structural components, comprising the clamping beam, distribution beam, spherical hinge, force sensor, lever, specimen, pin, counter-weight basket, and pendulum, are modelled with eight-node solid elements (SOLID). The reinforcing bars are modelled with two-node Hughes–Liu beam elements (BEAM), whilst the prestressed rods (32 mm diameter) and counterweight steel cables (30 mm diameter) are represented using discrete beam/cable elements (DISCRETE BEAM/CABLE). A mesh sensitivity analysis was conducted to guarantee simulation accuracy, yielding a consistent element size of 25 mm for both the reinforcement and the concrete. Fig. 1(b) depicts the comprehensive finite-element model.

Mesh sensitivity and discretization. To justify the adopted discretization, a mesh sensitivity check was performed by refining and coarsening the concrete and reinforcement meshes and monitoring the stability of key response metrics (e.g., peak impact force and peak lateral displacement at mid-height). The element size of 25 mm provides stable responses while maintaining reasonable computational efficiency and was therefore adopted for all subsequent simulations.

The steel reinforcement is modelled using the PIECE-WISE_LINEAR_PLASTICITY material model to replicate the mechanical behavior of the longitudinal and transverse reinforcement in RC columns subjected to impact loads. The constitutive relationship of steel was defined based on the stress–strain data obtained from uniaxial tensile testing, as outlined by Sun et al. [11]. This model encompasses the elastic–plastic behaviour of the steel and incorporates strain-rate effects and material failure mechanisms. The critical parameters C and P are established at 7.274 × 107 and 11.22, respectively; the mass density ρ is 7850 kg/m³, Young's modulus E is 206 GPa, and Poisson's ratio μ is 0.3, with supplementary parameters referenced from Fan et al. [20].

In this study, C and P are strain-rate parameters used to characterize the rate-dependent behavior of concrete under dynamic loading conditions. Parameter C governs the magnitude of strength enhancement induced by increasing strain rate, while P controls the sensitivity of the material response to changes in strain rate. These parameters are introduced to properly capture the dynamic increase effect of concrete in the finite element simulations and are kept consistent throughout the analysis. The material parameters for the reinforcement in the foundation beam and column cap were identical to those used for the columns, as delineated by Sun et al. [12].

The concrete is represented utilising the Continuous Surface Cap Model (CSCM), which is widely used to depict the constitutive behavior of concrete under low-velocity impact loading [21-23]. This model accounts for material damage, softening, degradation of elastic modulus, volumetric plasticity, and strain-rate sensitivity. In this study, the RC columns are modeled using user-defined parameters in accordance with the CSCM-159 requirements, with the comprehensive parameter set specified by Sun et al. [12].

The pendulum hammer, reaction-frame pin, reaction frame, force sensor, spherical hinge, distribution beam, and clamping beam are treated as ELASTIC materials, with $\rho = 7850$ kg/m³, $E = 206$ GPa, and $\mu = 0.3$. The pendulum counterweight is defined as a RIGID material, with its mass density determined from the actual mass and volume. The remaining components

employ the same material conventions as outlined in Sun et al. [12]. Contact interactions among components are established utilising the AUTO_SURFACE_TO_SURFACE keyword, with a friction coefficient of 0.02 between the clamping beam and the column cap. The reaction frame, steel cables, and counterweights are linked at coincident nodes. The reaction-frame pins are designated with specified restrictions. Specifically, the base and the terminus of the clamping beam are restricted in the Y and X/Y directions, respectively. In contrast, all eight apertures at the base of the foundation beam are subjected to entirely fixed boundary restrictions.

Contact and boundary condition idealization. All components interactions are defined using the AUTO_SURFACE_TO_SURFACE contact formulation. A low friction coefficient (0.02) is assigned to the clamping beam-column cap interface to represent the low-friction steel-concrete contact and to remain consistent with the validated modelling strategy reported by Sun et al. [12]. Boundary constraints are idealized directly from the test setup in Fig. 1(a). The reaction-frame/pin system restrains the column cap to allow axial deformation while preventing transverse motion. Meanwhile, the foundation beam is fully fixed at the anchor-bolt holes to represent the rigid connection to the strong floor. These modeling assumptions reproduce the experimental load path and improve the transparency and reproducibility of the numerical model.

2.3. Model validation

The FE model is validated against experimental data obtained from controlled pendulum impact tests reported by Ref. [11]. The experimental program provides measured impact force histories, lateral displacement responses, and observed damage patterns of RC columns subjected to lateral impact loading. These experimental results are used as benchmark data to evalute the accuracy and reliability of the proposed FE model. Figs. 2 to 4 juxtapose the finite element simulation outcomes with empirical data. Fig. 2 demonstrates that the simulated impact-force time histories align closely with the data, exhibiting only minor discrepancies in peak impact force and several characteristic points. This agreement indicates that the FE model can effectively capture the impact-force response of the specimens. Fig. 3 compares the measured and simulated lateral displacement time histories at the impact location (mid-height). The results show that the FE model reproduces the overall deformation development of the specimens throughout the impact process.

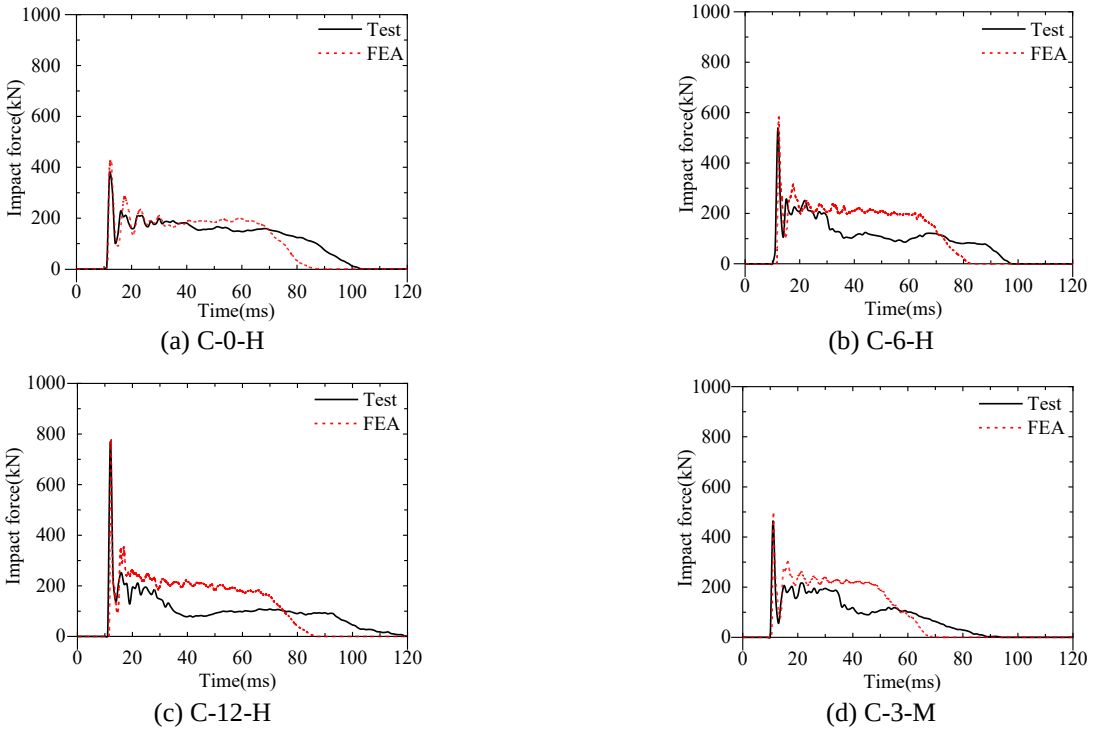

(a) C-0-H (b) C-6-H

(c) C-12-H (d) C-3-M

Fig. 2 Comparison of test and finite element simulated impact forces

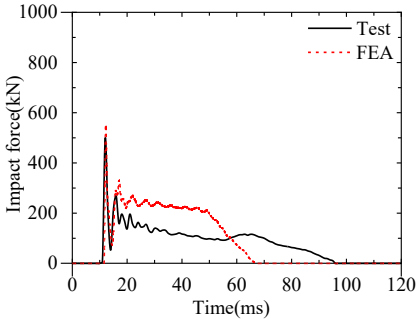

(e) C-6-M

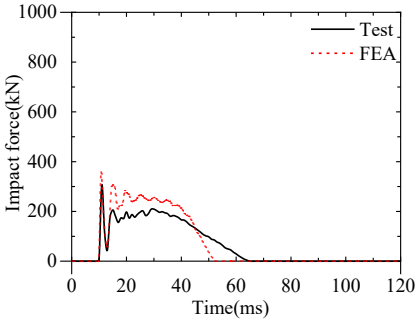

(f) C-6-L

Fig. 2 Comparison of test and finite element simulated impact forces (continued)

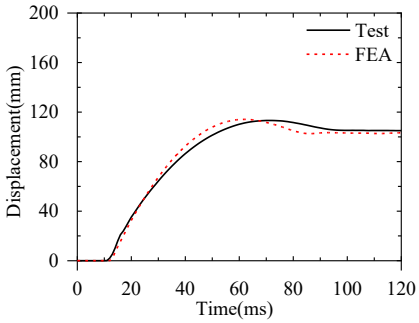

(a) C-0-H

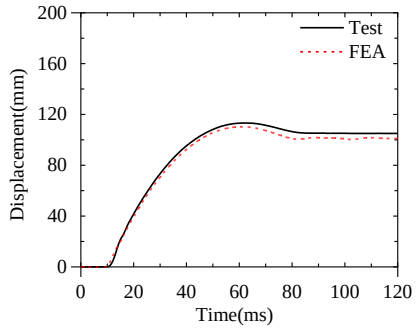

(b) C-6-H

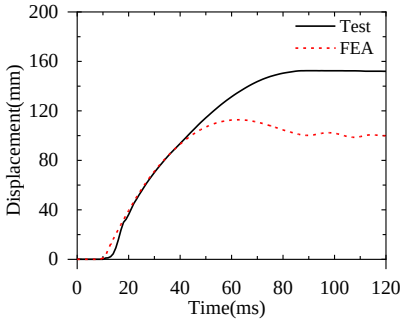

(c) C-12-H

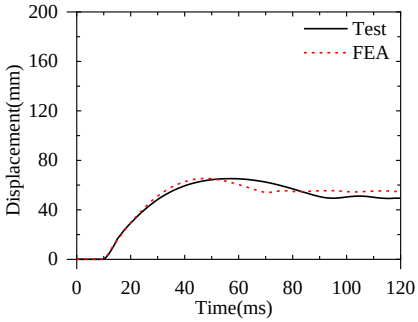

(d) C-3-M

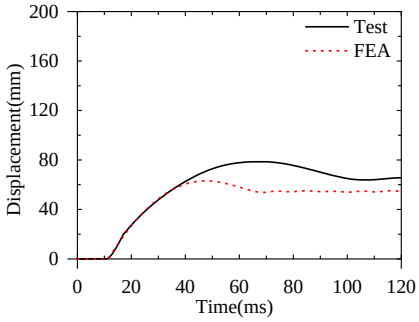

(e) C-6-M

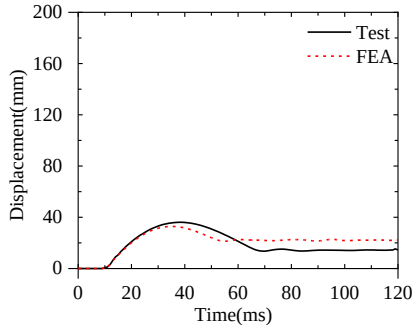

(f) C-6-L

Fig. 3 Comparison of test and finite element simulated lateral displacements

The general trend of the simulation results agrees well with the experimental observations, with only slight discrepancies at certain time intervals. Fig. 4 compares the predicted failure modes with the actual outcomes, illustrating that the simulation yields plausible predictions of crack distribution, propagation, and primary damage zones, consistent with the experiments. Collectively, these findings demonstrate that the finite-element model exhibits robust predictive capabilities for impact force, displacement, axial force, and damage distribution. The model effectively represents the dynamic response and failure mechanisms of RC columns subjected to lateral impact. It consequently offers a dependable numerical foundation for subsequent parametric analyses and investigations of shear-failure causes.

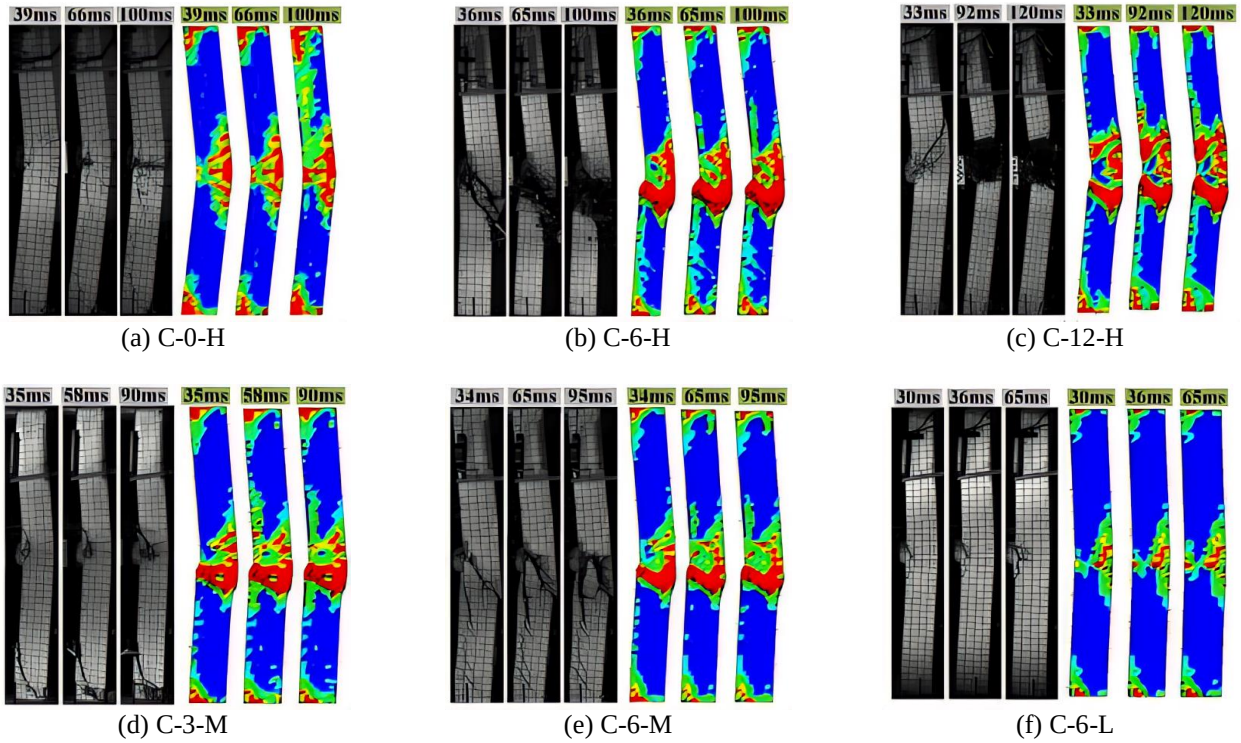

(a) C-0-H (b) C-6-H (c) C-12-H

(d) C-3-M (e) C-6-M (f) C-6-L

Fig. 4 Comparison of experimental damage patterns and numerical damage predictions

3. Discussion on Shear Mechanisms of RC Columns

This section investigates the characteristics of shear force distribution in RC columns subjected to lateral impact. The analysis focuses on the variations in shear force along the column height during the impact loading phase. Such understanding is crucial for comprehending the transition from flexural-dominated responses to shear-giverned failure. By examining the evolution of these forces, the study provides key insights into the dynamic behavior of RC columns, thereby informing the development of impact-resistant design strategies.

3.1. Characteristics of shear force distribution

Fig. 5 illustrates shear-force distribution curves along the column height at different intervals preceding the peak response. The maximum shear force near the impact site coincides almost simultaneously with the peak impact force during the initial loading phase, similar to the inertia-force distribution. The shear-force distribution varies significantly during loading, and the combined effects of impact and inertia forces result in substantial alterations in the location and timing of the peak shear force.

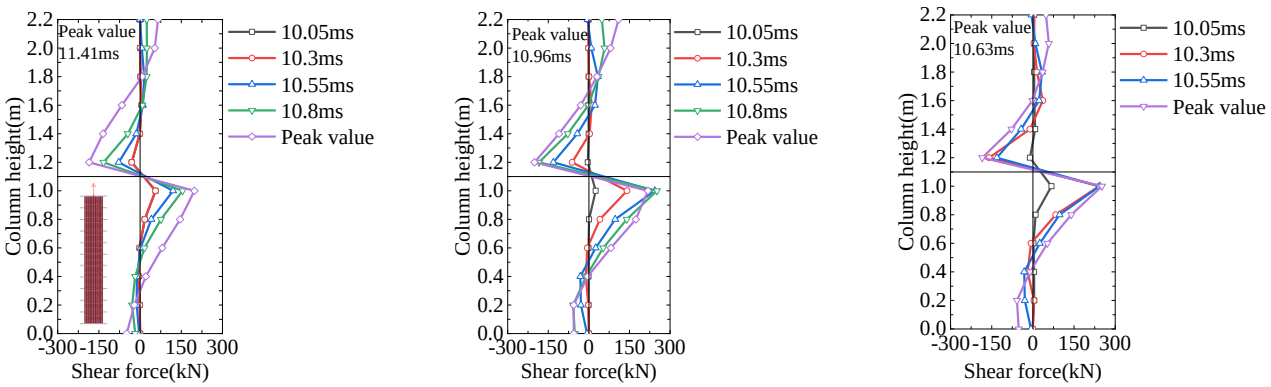

(a) C-0-H (b) C-6-H (c) C-12-H

Fig. 5 Pre-peak shear force along column height

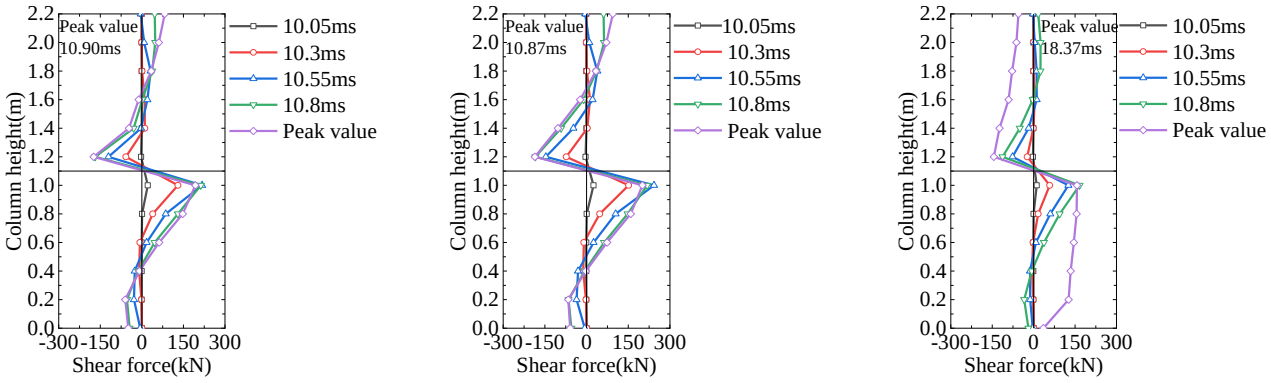

(d) C-3-M (e) C-6-M (f) C-6-L

Fig. 5 Pre-peak shear force along column height (continued)

The shear-force profile in RC columns under impact loading differs substantially from that under static loading, resulting in distinct failure modes. Before the peak, each column demonstrates a comparable pattern: an abrupt alteration and sign reversal of the shear force near the impact point, where shear forces significantly surpass those at other sections. In contrast, the shear forces at the column ends remain considerably lower.

In columns demonstrating shear failure, the peak shear force is attained sooner than in specimens showing flexural failure, and occurs even earlier as the axial compression ratio increases. Consequently, the rate of shear-force development is more pronounced in shear-failed columns (C-6-H, C-12-H, C-3-M, and C-6-M) compared to those with flexural failure. At the peak response, increasing the axial compression ratio from 0 to 0.64 raises the shear force from 159.1 kN to 255.36 kN (60.5 %), whilst boosting the impact velocity from 2.58 m/s to 4.58 m/s raises the shear force from 134.4 kN to 251.9 kN (87.4 %). These results demonstrate that increased axial compression ratios and greater impact velocities substantially improve the peak shear force in the columns.

3.2 Characteristics of bending moment distribution

Only the distribution of the bending moment during the early phase before its peak is addressed, as it stabilizes thereafter. Fig. 6 illustrates the pre-peak bending-moment distribution curves, whereas Table 1 compares the shear force and bending moment at the time of peak response. During the early phase of impact, each column segment experiences a specific magnitude of negative bending moment. The location of zero bending moment progressively moves towards the column end as time progresses, ultimately reaching the end when the peak is approached. At this juncture, the bending-moment distribution stabilizes and closely resembles that under static loading.

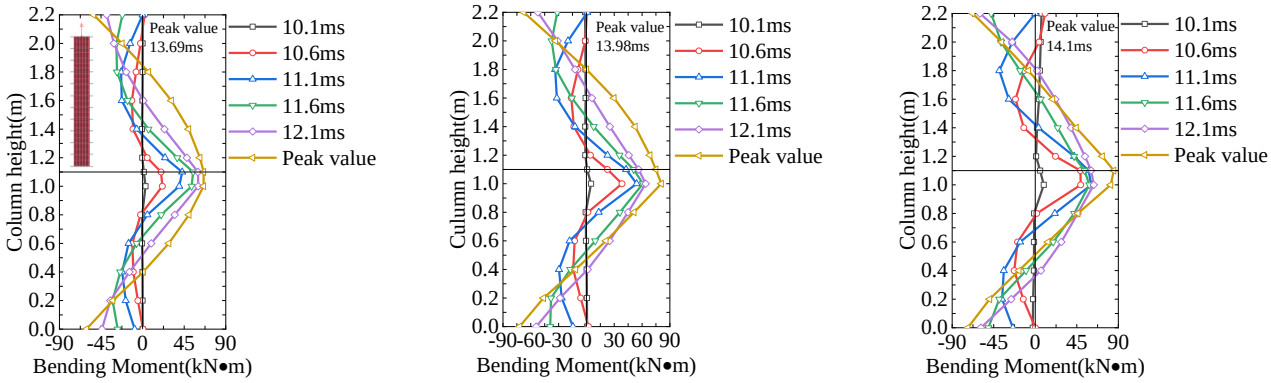

(a) C-0-H (b) C-6-H (c) C-12-H

Fig. 6 Pre-peak bending moment along column height

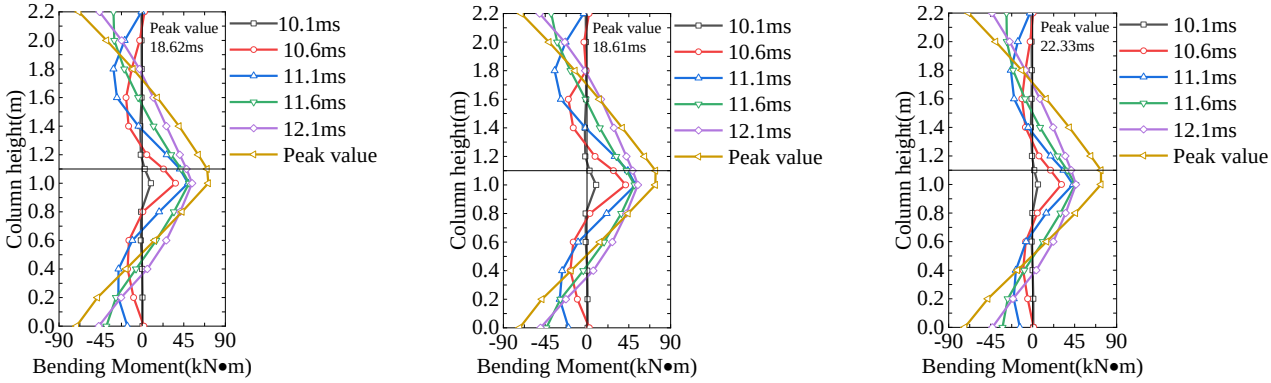

(d) C-3-M (e) C-6-M (f) C-6-L

Fig. 6 Pre-peak bending moment along column height (continued)

Table 1 Comparison of peak shear forces and bending moments

No.	Peak Shear Force (kN)	Improvement (%)	ΔS C-6-L(%)	Peak Moment (kN·m)	Improvement (%)	ΔM C-6-L(%)	M/S* Ratio
C-0-	159.1	-		62.1	-		0.390
C-6-	251.9	+58.3	+87.4	80.8	+30.1	+29.1	0.321
C-	255.3	+60.5		74.9	+20.6		0.293
C-3-	193.1	-		70.3	-		0.364
C-6-	218.1	+12.9	+62.3%	73.8	+5.0	+17.9	0.338
C-6-	134.4	-		62.6	-		0.466

* Moment/Shear.

In contrast to static loading, however, both positive and negative bending moments coincide at impact: positive moments at the point location and negative moments at the column ends, with the magnitudes of the stabilized positive and negative moments being approximately equal. Fluctuations in bending moments across time and place due to various impact scenarios might result in unique failure modes. Analysis of bending-moment progression reveals that in the initial phase of impact (before the peak), the activated length of the column constitutes approximately one-third of the total height. As the inertia force propagates to the column end, its distribution along the RC column alters considerably, generating higher-order vibration modes that subsequently influence the shape of the bending-moment distribution.

With the increase in both the axial compression ratio and impact velocity, there is a significant rise in the positive bending moment at the impact location and the negative bending moment at the column extremities, with the effect being more pronounced at higher axial compression ratios. At an impact velocity of 3.58 m/s, augmenting the axial compression ratio from 0.16 to 0.32 elevates the peak bending moment from 70.3 kN·m to 73.8 kN·m, indicating a 5.0% increase. Maintaining an impact velocity of 4.58 m/s elevates the peak bending moment from 62.1 kN·m to 74.9 kN·m, representing an increase of 20.6%. When the axial compression ratio is maintained at 0.32, increasing the impact velocity from 2.58 m/s to 4.58 m/s raises the peak bending moment from 62.6 kN·m to 80.8 kN·m, representing a 29.1% increase.

These findings indicate that both impact velocity and axial compression ratio significantly affect the structural response of RC columns. Conversely, when the axial compression ratio is 0.32, the increase in peak bending moment (30.1%) is greater than that observed at an axial compression ratio of 0.64. This discrepancy occurs because, at elevated axial compression ratios,

the column's flexural capacity approaches its limit, resulting in diminished effects of further increases in compression ratio on impact enhancement. Consequently, in practical engineering applications, effectively regulating the axial compression ratio can be a more efficient approach to enhancing the structural resilience of RC columns to impact loading.

It is noted that as the axial compression ratio increases from 0 to 0.64, the timing of the peak bending moment is postponed, extending from 13.69 ms to 14.1 ms. Conversely, augmenting the impact velocity from 2.58 m/s to 4.58 m/s reduces the time to peak from 22.33 ms to 13.98 ms. This phenomenon can be elucidated from two viewpoints. An elevated axial compression ratio enhances the total flexural rigidity of the column. The development of bending moments necessitates the whole response of the column; thus, enhanced stiffness postpones the peak bending moment. Secondly, an increased impact velocity enhances the dynamic response of the column, resulting in a more rapid transmission of the impact force and, therefore, an earlier peak bending moment.

3.3. Characteristics of critical surface loading

For RC columns demonstrating shear failure (C-6-H and C-12-H), the critical section is identified at the midpoint of the diagonal crack. The precise site of flexural failure was determined for columns C-0-H and C-6-L. Time histories of shear force and bending moment are plotted at these critical locations along the column height. Fig. 7 illustrates the shear and moment histories at these critical sections under impact. The shear-force time history at the critical section roughly follows the impact-force time history; however, the peak shear force is considerably lower than the peak impact force. The peak bending moment typically arises after the peak shear force because the shear force, once established, exerts immediate influence on the column and disseminates swiftly through it via shear mechanisms along a more concise transfer path, facilitating the peak to form earlier. In contrast, bending moments arise from alterations in column curvature and require the response of the entire column, leading to a delayed peak. These observations highlight the necessity of evaluating shear force and bending moment concurrently in the design of RC columns to guarantee stability and safety under impact loads.

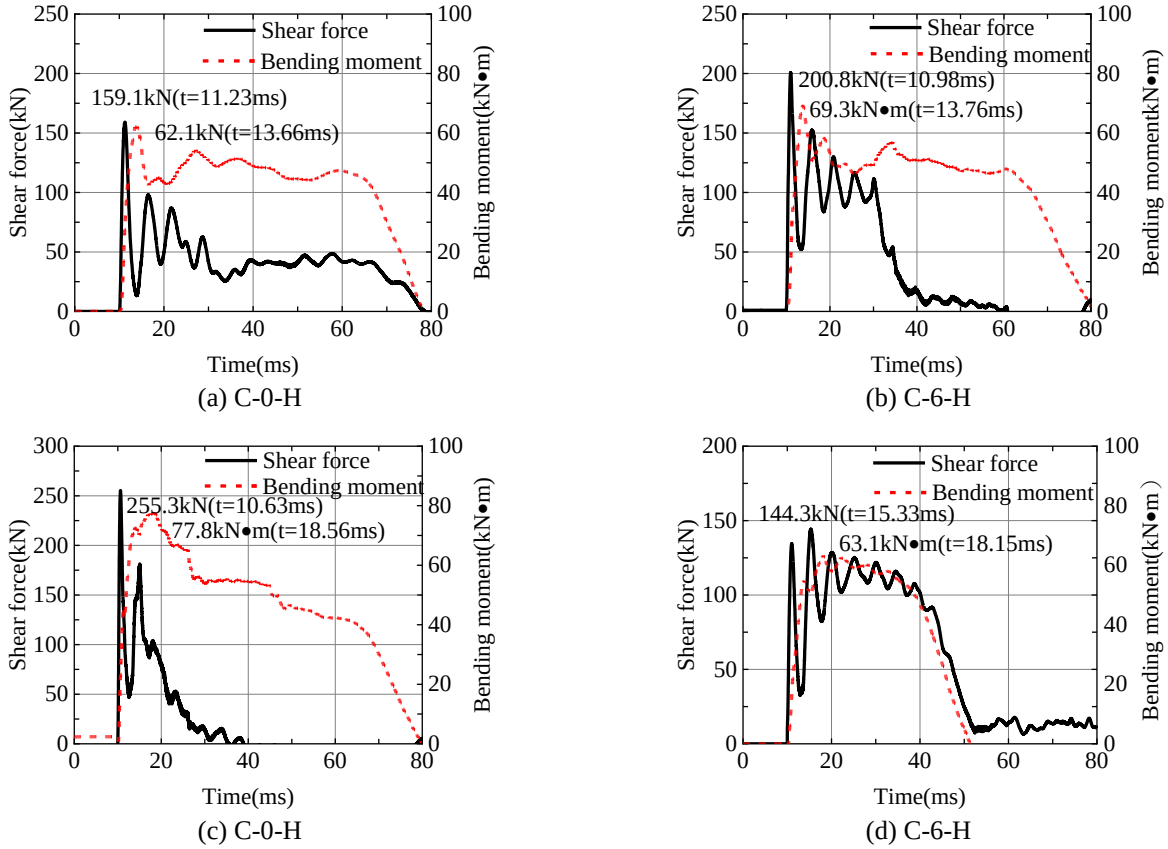

Fig. 7 Shear and moment histories at critical sections under impact

Fig. 8 illustrates the integrated loading trajectories of bending moment and shear force at the critical sections of columns, demonstrating flexural and shear failure. Analogous to RC beams [24], the relationship between shear force and bending moment in RC columns under impact loading is intricate and significantly diverges from static behavior. During the initial phase of impact, both shear force and bending moment increase rapidly and concurrently. The shear force is substantial, while the bending moment is minor, leading to a significant delay in the progression of the bending moment. At this moment, the ratio of bending moment to shear force is lower than at the corresponding section under static loading, but it progressively rises with time.

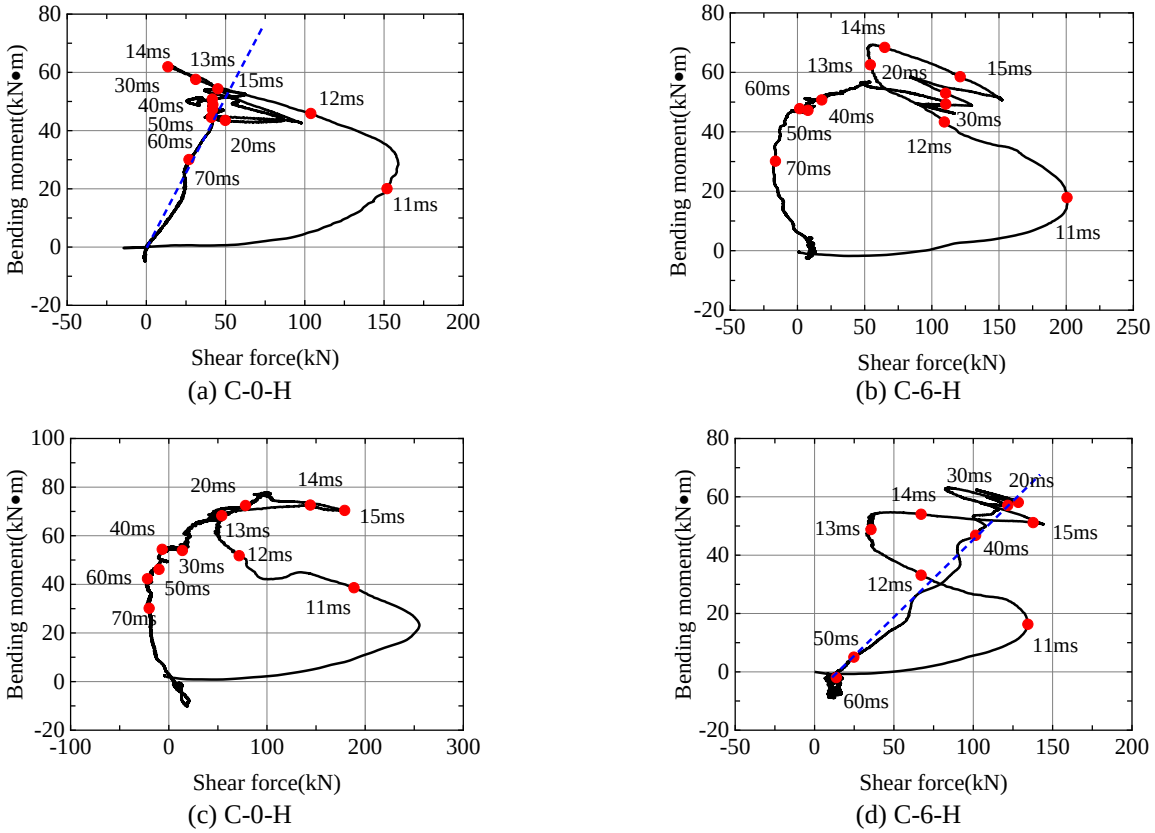

Fig. 8 Moment-shear path evolution under cyclic loading

As shown in Fig. 8, during the later stages of impact, notable distinctions emerge between columns experiencing flexural failure and those undergoing shear failure. In flexural failure columns, the ratio of bending moment to shear force approximates that of static loading and remains relatively stable during the post-impact phase, indicating that overall deformation may evolve to resemble static conditions. Conversely, in columns exhibiting shear failure, this ratio does not maintain constancy, contrasting sharply with the behavior of RC beams subjected to shear failure [25]. Following shear failure, the axial force significantly impacts the column, and the ensuing *P–δ* effect (additional moments induced by lateral displacements) becomes dominant, affecting the magnitudes of both bending moment and shear force. The predominant impact of axial force and the *P–δ* effect underscores the intricacy of shear-failure mechanisms in RC columns.

In the preliminary phase of impact, comparison of specimens C-0-H, C-12-H, and C-6-H shows that the M–V trajectories diverge as the axial compression ratio increases. The noted outward expansion indicates that elevated axial compression ratios increase the columns' vulnerability to shear failure, which is consistent with experimental observations. Furthermore, due to the early occurrence of shear failure during impact, the M–V trajectory gradually deviates from the proportional path observed under static loading. The interaction between shear force and bending moment significantly affects the impact performance of RC columns. Therefore, tracking the onset of shear failure and its influence on the evolution of the M–V trajectory is essential for improving the impact resistance of RC columns, especially under high axial compression ratios.

4. Parametric Analysis

The limited parameter range in the experimental program motivates this parametric study. Base on validated finite element model and the previously discussed failure mechanisms, this section investigates the influence of several key parameters—including impact mass-velocity combinations, stirrup ratio, slenderness ratio, axial compression ratio, longitudinal reinforcement ratio, and concrete strength—on the dynamic response and failure modes transition of RC columns subjected to lateral impact. The selection and analysis of these factors follow the modelling approach described in reference [12].

4.1. Impact mass-velocity combinations

Figs. 9 and 10 illustrate the dynamic response trends and the progression of failure modes for Group B columns (i.e., the specimens in Ref. [11] with the same geometry and reinforcement configuration, tested under different impact mass–velocity combinations in order to isolate the influence of impact scenarios). In these experiments, the impact mass decreases from 2,667 kg to 667 kg, but the impact velocity increases from 2.71 m/s to 15.71 m/s, culminating in a rise in impact energy from 8.4 kJ to 36.4 kJ. As shown in Fig. 10, when impact velocity increases, both impact force and contact length escalate exponentially, rising by 259.9% and 51.7%, respectively. In contrast, the peak displacement at the impact point and the residual displacement increase linearly by 718.2% and 1,609.7%, respectively, indicating that the displacements escalate substantially more than the impact force. Fig. 10 demonstrates that, at lower impact velocities, RC columns are more likely to exhibit a flexural failure, marked by relatively uniform crack distribution and incomplete horizontal cracks.

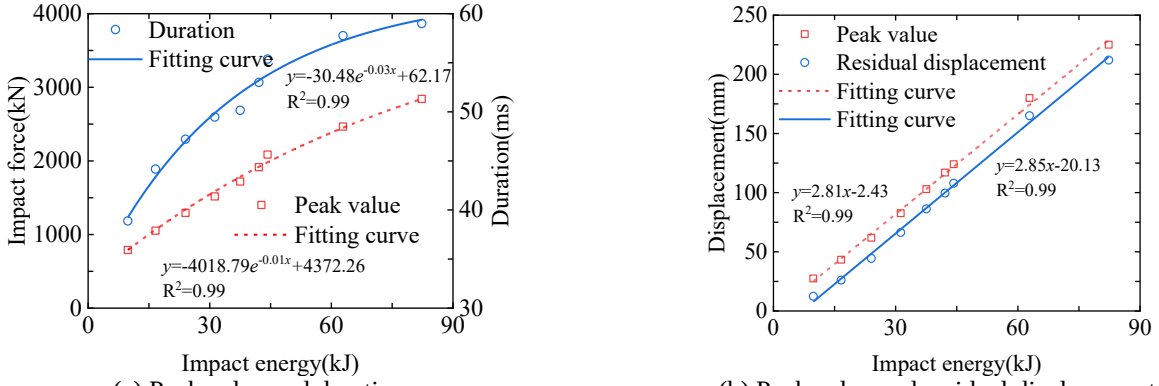

(a) Peak value and duration (b) Peak value and residual displacement

Fig. 9 Impact force and displacement with different impact energie

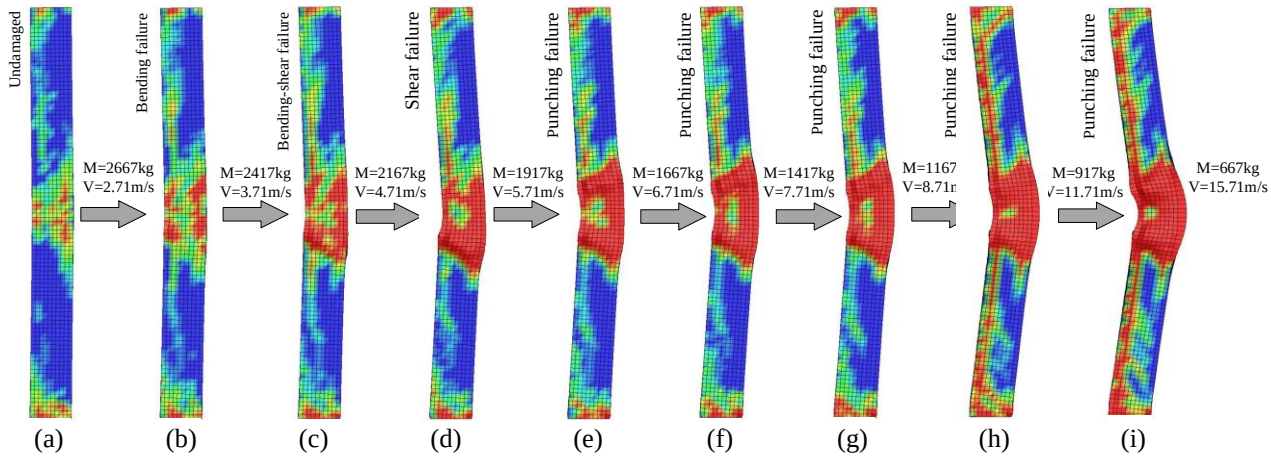

Fig. 10 Failure mode transition thresholds under varying impact energy:

At elevated impact velocities, the concrete in the contact area is fragmented, and horizontal fissures decrease. Diagonal fractures accumulate around the impact zone and swiftly extend from the tension side toward the compression side, diminishing the localised load-bearing capability. As impact velocity rises, the quantity and severity of diagonal cracks further expand. Upon reaching a velocity of 6.71 m/s, additional increments result in a reduction of diagonal fracture propagation, with cracks extending at roughly 45° toward the tension side and forming shear keys. As these diagonal fissures progress, the shear key is ultimately freed from the column. When the reinforcement at the impact region reaches its tensile strength and the concrete in the compression zone fractures, a plastic hinge develops, causing the displacement at the impact point to cease converging. Accordingly, as impact energy increases, the failure mode evolves through the following sequence: no failure→flexural failure →flexure–shear failure→shear failure→punching shear failure.

4.2. Stirrup ratio

The stirrup spacing is decreased from 150 mm to 25 mm, resulting in an increase in the ratio from 0.38% to 2.28%. The impact mass is kept constant at 2,167 kg, and the impact velocity at 4.71 m/s. Fig. 11(a) demonstrates that the peak impact force escalates linearly as the stirrup ratio rises because the column's local resistance dictates the peak force. An elevated stirrup ratio improves local shear stiffness, thereby augmenting the peak force. Conversely, the duration of impact diminishes exponentially with increasing stirrup ratio, likely due to increased stirrups constraining the deformation of concrete, resulting in the rapid dissipation of impact energy. Fig. 11(b) illustrates that both the peak and residual displacements at the impact point decrease exponentially as the stirrup ratio increases, signifying a decreased deformation capacity and, thus, lower energy absorption.

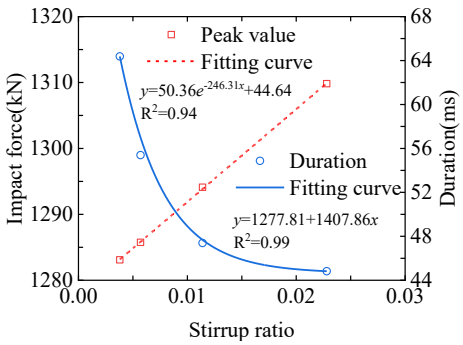

(a) Peak value and duration

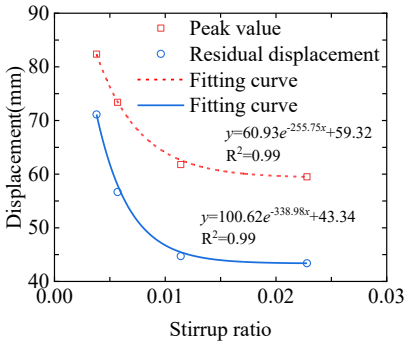

(b) Peak value and residual displacement

Fig. 11 Effect of stirrup ratio on impact force-displacement

Fig. 12 illustrates that augmenting the stirrup ratio minimally influences the development of horizontal cracks. As the stirrup ratio diminishes, diagonal fissures emerge in the vicinity of the contact area between the pendulum and the column, extending from the tensile side towards the impact location. As a result, with an increase in the stirrup ratio, the failure mode transitions from punching-shear failure to shear failure, flexure-shear failure, and ultimately flexural failure.

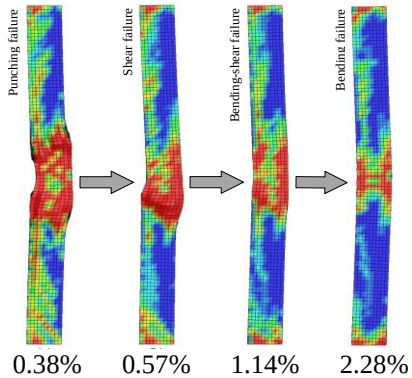

Fig. 12 Failure mode change with stirrup ratio

4.3. Slenderness ratio

The slenderness ratio is altered by increasing the column height from 2.0 m to 4.0 m while the pendulum mass remains constant at 2,167 kg and the impact velocity at 4.71 m/s; the reinforcement specifications are consistent with those of Group A. As a result, the slenderness ratio rose from 8 to 16. Figs. 13 and 14 illustrate variations in dynamic response and failure-mode transitions for columns exhibiting distinct slenderness ratios.

Fig. 13(a) illustrates that the peak impact force exhibits minimal variation with increasing slenderness ratio, because the slenderness ratio exerts negligible influence on local contact stiffness and can be considered inconsequential in this context. In contrast, the duration of impact increases linearly with the slenderness ratio. Fig. 13(b) illustrates that both the peak and residual displacements at the impact site grow exponentially with the slenderness ratio, signifying a decrease in the column's natural frequency. As the slenderness ratio increases, the increased mass involved in the column's response during impact facilitates more efficient absorption and dissipation of impact energy, resulting in bigger displacements. Fig. 14 illustrates that with an increase in the slenderness ratio, the failure mode transitions from shear failure to flexure–shear failure, ultimately culminating in flexural failure. The discovery that increased slenderness ratios result in larger displacements and a shift in failure mode highlights the influence of slenderness on energy dissipation and damage evolution in RC columns.

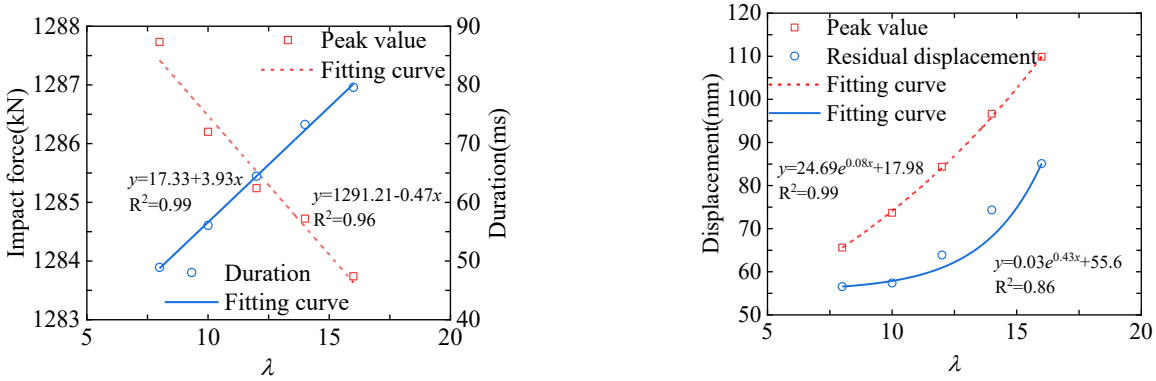

(a) Peak value and duration (b) Peak value and residual displacement

Fig. 13 Impact force and displacement in columns with various slenderness ratios

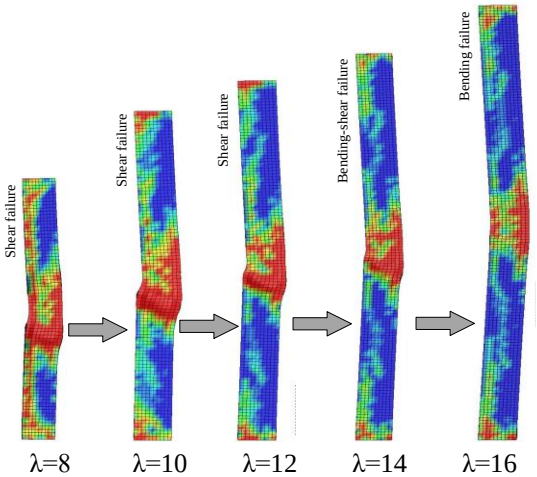

Fig. 14 Failure mechanism shift in slender columns under impact

4.4. Axial compression ratio

In this context, Group A columns refer to specimens group defined in the experimental program reported in Ref. [11]. These specimens share identical geometric dimensions and reinforcement details and are used as a reference group for comparison with other specimen groups under different impact conditions. Prior research demonstrates that augmenting axial

pressure enhances the performance of RC columns under impact loading [11, 26]. Figs. 15 and 16 present the dynamic response and failure-mode transitions of Group A columns with differing axial compression ratios, exposed to an impact mass of 2,167 kg and an impact velocity of 4.71 m/s. The axial load applied at the column top is modified by altering the mass density of the counterweight hung at the end of the lever. Fig. 15 (a) shows that augmenting the axial compression ratio from 0 to 0.64 raises the peak impact force from 1,216.5 kN to 1,334.7 kN (an increase of 9.72 %). The trend demonstrates exponential growth but decelerates at elevated compression ratios. This behavior occurs because the configuration of the first pulse of the impact force is influenced more by the increased contact stiffness between the pendulum and the column than by the overall stiffness of the structure.

According to Fig. 15(a), as the axial compression ratio escalates from 0 to 0.34, the impact duration rises from 51.78 ms to 55.01 ms (an increase of 6.23 %). Further increasing the ratio from 0.34 to 0.64 reduces the duration from 55.01 ms to 53.23 ms (a reduction of 3.23%), demonstrating that the impact duration initially rises and subsequently declines with the axial compression ratio, exhibiting a quadratic trend. Fig. 15(b) illustrates that augmenting the axial compression ratio from 0 to 0.64 diminishes the peak and residual displacements at the impact point by 15.7 % and 17.9 %, respectively, signifying that a higher axial compression ratio enhances the overall stiffness of the column during the first response cycle. In subsequent later stages of impact, the P–δ effect becomes significant, resulting in increased lateral displacement. Fig. 15(b) demonstrates that when the axial compression ratio surpasses 0.24, the influence of axial load on residual displacement becomes insignificant. This occurs primarily due to the enhanced lateral stiffness, which attenuates the free-vibration response.

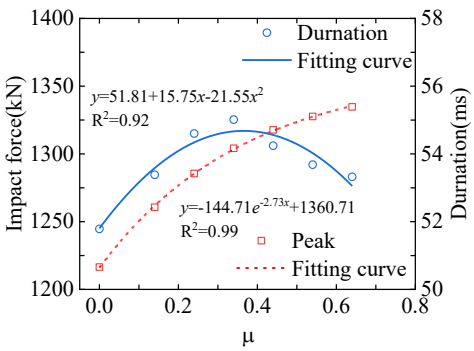

(a) Peak value and duration

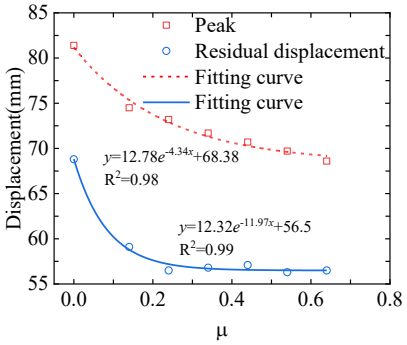

(b) Peak value and residual displacement

Fig. 15 Impact response trends under different axial compression ratios

Fig. 16 illustrates that with increasing axial compression ratio, significant diagonal cracks develop in the impact zone. Augmented axial pressure generally mitigates tensile damage in the concrete, thereby restricting the proliferation of diagonal cracks. Consequently, axial pressure mitigates concrete cracking and influences the failure mode of the concrete. When the axial compression ratio is zero, cracking predominantly appears as horizontal and diagonal fissures. With an increase in the axial compression ratio, the failure mode shifts from flexure–shear failure to pure shear failure.

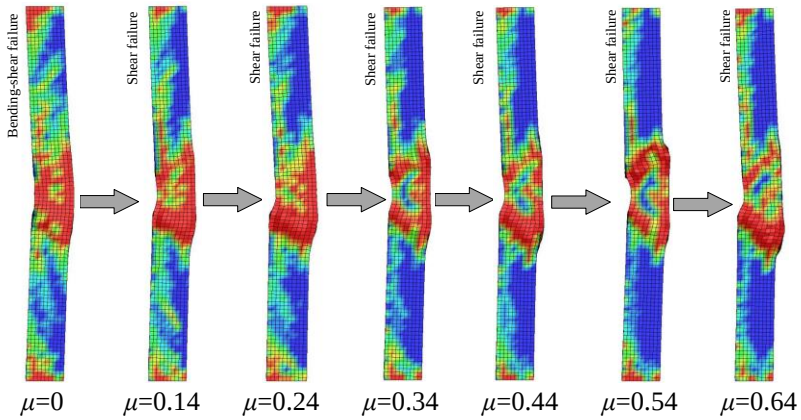

Fig. 16 Failure mode shift with axial compression ratio

4.5. Longitudinal reinforcement ratio

The diameter of the longitudinal bars is modified in accordance with the Group B configuration to adapt the longitudinal reinforcement ratio. Diameters vary from 14 mm to 25 mm, with reinforcement ratios ranging from 0.99 % to 2.51 %. The impact mass is set at 2,167 kg, and the impact velocity at 5.71 m/s. Figs. 17 and 18 illustrate the impact of varying longitudinal reinforcement ratios on the dynamic response and failure-mode transitions of the columns. Fig. 17(a) demonstrates that the peak impact force escalates exponentially with an increase in the longitudinal reinforcement ratio, whereas the impact duration diminishes exponentially. Fig. 17(b) illustrates that both the peak and residual displacements at the impact point also decrease exponentially with increasing reinforcement ratio. The results demonstrate that the time of contact duration between the pendulum and the column is intricately linked to the structure's deformation capacity and stiffness.

Moreover, augmenting the diameter of the tensile reinforcement enhances the overall stiffness of the column, substantially enhancing impact resistance. Fig. 18 shows that the number of horizontal and diagonal cracks diminishes with an increase in the longitudinal reinforcement ratio. The longitudinal reinforcement ratio significantly affects the level of damage incurred by the column. The significant effect of the reinforcement ratio may be attributed to the fact that, during the initial phase of impact, the majority of the impact energy is absorbed by the concrete. Conversely, at subsequent stages, the reinforcement plays a more critical function in mitigating the effect [27]. As a result, an increase in the longitudinal reinforcement ratio causes the failure mode to shift from flexural failure to flexure–shear failure and finally to punching-shear failure.

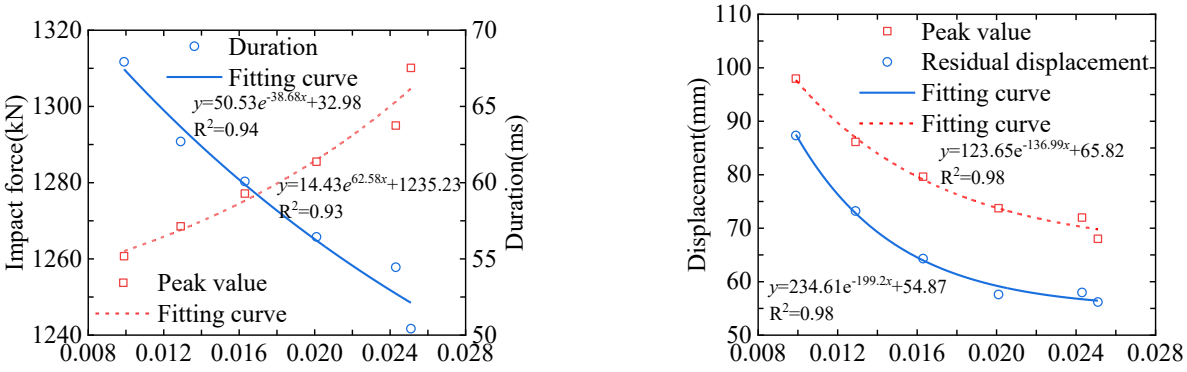

(a) Peak value and duration (b) Peak value and residual displacement

Fig. 17 Influence of longitudinal reinforcement ratio on impact force-displacement

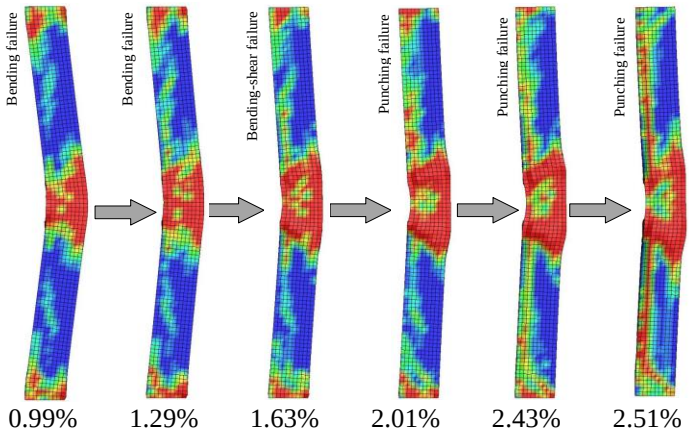

Fig. 18 Failure mode transition with varying reinforcement ratio

4.6. Concrete strength

This study examines the influence of concrete strength on the dynamic response and failure-mode transitions of RC columns. The compressive strength varies from 28 MPa to 78 MPa, while the reinforcement configuration follows that of

Group B. The impact mass is fixed at 2,167 kg, and the impact velocity is set to 6.71 m/s. As shown in Fig. 19, increasing concrete strength reduces the impact duration as well as the peak and residual displacements at the impact point. Figs. 19 and 20 further illustrate the effects of concrete strength on the dynamic response and the progression of failure modes. Fig. 20(a) shows that increasing the concrete strength from 28 MPa to 78 MPa raises the peak impact force from 1,728.1 kN to 2,166.9 kN (a 22.5% increase). This is primarily because a higher elastic modulus elevates the contact stiffness between the pendulum and the column. These reductions in displacement and duration are explained by differences in energy absorption: under a constant total energy input, lower-strength columns—with lower stiffness—undergo greater plastic deformation and thus absorb and dissipate more impact energy. Fig. 20 also indicates a larger volume of plasticized concrete in the lower-strength specimens, underscoring the substantial influence of concrete strength on failure mode. When the strength is below 38 MPa, the columns predominantly exhibit shear cracks inclined at less than 45°, characteristic of punching-shear failure. As the concrete strength increases, the failure mode gradually transitions from punching-shear failure to shear-dominated behaviour and eventually to flexural failure.

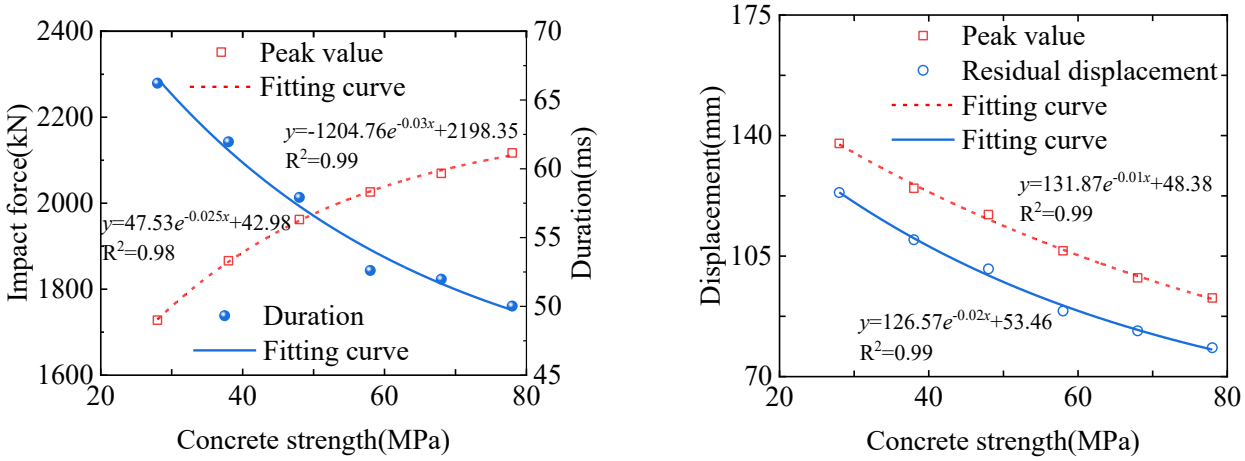

(a) Peak value and duration (b) Peak value and residual displacement

Fig. 19 Effect of concrete strength on impact response

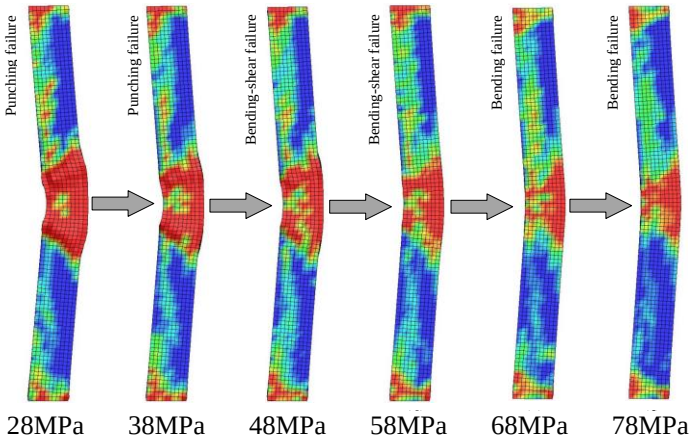

Fig. 20 Failure mode transformation with increasing concrete strength

4.7. Engineering design implications

To improve the practical relevance of the numerical findings, the key design implications for RC columns subjected to lateral impact are summarized as follows:

(1) Transverse reinforcement: Increasing the stirrup ratio effectively delays diagonal shear cracking and shifts the failure mode from brittle shear toward flexure or flexure–shear. Therefore, adequate transverse reinforcement and confinement detailing are critical for columns susceptible to impact.

(2) Axial compression level: While moderate axial compression can increase initial resistance, excessive axial compression accelerates shear damage development and reduces deformation capacity. Impact-resistant design should avoid overly high axial compression ratios or provide enhanced shear detailing when high axial loads are unavoidable.

(3) Slenderness and flexural demand: Columns with larger slenderness ratios tend to exhibit greater lateral displacements and more flexure-dominated responses. Both shear capacity and displacement demand should be checked in tandem, particularly for short or stocky columns where shear-governed failures are more likely.

(4) Longitudinal reinforcement and local damage: Higher longitudinal reinforcement ratios increase stiffness and reduce peak and residual displacements. However, they may also promote localized damage (e.g., punching-shear-type behavior) under severe impact. Balanced longitudinal–transverse reinforcement and local strengthening in the impact region are recommended.

(5) Impact scenario definition: Different impact mass–velocity combinations can produce distinct response characteristics even at similar impact energy. Design scenarios should consider representative mass, velocity, and contact duration/impulse rather than energy alone.

These recommendations provide a concise linkage between the numerical results and design-oriented considerations for improving the impact resilience of RC columns.

5. Conclusions

This study rigorously examined the dynamic response and shear failure mechanisms of RC columns under lateral impact using experimental tests and finite element simulations. Unlike recent studies (including Sun et al. and others) that primarily reported global response indices or limited parameter variations, this study provided a mechanism-driven understanding of impact-induced shear failure, quantified failure-mode transitions across multiple key parameters, and clarified the shear–moment interaction under impact loading. The main conclusions are summarized as follows:

(1) RC columns exposed to lateral impact exhibit inertia-induced diagonal cracks that spread swiftly, resulting in a shift from flexural to brittle shear-dominated failure modes.

(2) Elevated axial compression ratios and increased impact velocities markedly exacerbate shear failure, increasing shear pressures and diminishing deformation capacities.

(3) Augmenting the stirrup ratio and concrete compressive strength significantly postpones the initiation of shear cracking, enhances structural ductility, and improves overall impact resistance of RC columns.

(4) Columns exhibiting higher slenderness ratios undergo increased lateral displacements and reveal a distinct transition in failure mode from shear-dominated to flexure-dominated behavior.

(5) Increased longitudinal reinforcement ratios enhance structural stiffness and markedly decrease both peak and residual displacements, hence affecting the shift from flexural failure towards punching-shear failure.

(6) In light of these findings, practical solutions are provided to improve the impact resistance of RC columns in engineering applications, including the regulation of slenderness ratios, the provision of sufficient stirrup reinforcement, and the precise assessment of likely impact scenarios.

Conflicts of Interest

The authors declare no conflict of interest.

References

[1] B. Li, E. S. S. Lam, B. Wu, and Y. Y. Wang, “Effect of High Axial Load on Seismic Behavior of Reinforced Concrete Beam-Column Joints with and without Strengthening,” ACI Structural Journal, vol. 112, no. 6, pp. 713-724, 2015.

[2] F. Faleschini, P. Bragolusi, M. A. Zanini, P. Zampieri, and C. Pellegrino, "Experimental and Numerical Investigation on the Cyclic Behavior of RC Beam Column Joints with EAF Slag Concrete," Engineering Structures, vol. 152, no. 1, pp. 335-347, 2017.

[3] J. Li, R. Zhang, L. Jin, D. Lan, and Xiuli Du, "Simplified Support Reaction Profiles of RC Beams under Low-Velocity Impact: From Experimental Observations to Data-Driven Prediction," Engineering Structures, vol. 344, no. 1, article no. 121377, 2025.

[4] X. H. Bao, D. Li, D. Zhao, J. Shen, X. Chen, and H. Cui, "Lateral Impact Responses of Inclined Steel-Reinforced Concrete Column: Experimental and Numerical Investigations," Structures, vol. 74, article no. 108601, pp. 1-21, 2025.

[5] J. Sagaseta, P. Olmati, K. Micallef, and D. Cormie, "Punching Shear Failure in Blast-Loaded RC Slabs and Panels," Engineering Structures, vol. 147, pp. 177-194, 2017.

[6] M. Nagata, M. Beppu, H. Ichino, and J. Takahashi, "Method for Evaluating the Displacement Response of RC Beams Subjected to Close-In Explosion Using Modified SDOF Model," Engineering Structures, vol. 157, pp. 105-118, 2018.

[7] C. Zhang, G. Gholipour, and A. A. Mousavi, "State-of-the-Art Review on Responses of RC Structures Subjected to Lateral Impact Loads," Archives of Computational Methods in Engineering, vol. 28, pp. 2477-2507, 2021.

[8] X. Zhou, M. Zhou, D. Luo, B. Wu, and L. Liu, "Study on the Nonlinear Response and Shear Behavior of RC Columns under Lateral Impact," Structures, vol. 34, no. 4, pp. 3834-3850, 2021.

[9] S. El-Tawil, E. Severino, and P. Fonseca, "Vehicle Collision with Bridge Piers," Journal of Bridge Engineering, vol. 10, no. 3, pp. 345-353, 2005.

[10] N. Kishi, H. Mikami, K. G. Matsuoka, and T. Ando, "Impact Behavior of Shear-Failure-Type RC Beams without Shear Rebar," International Journal of Impact Engineering, vol. 27, no. 9, pp. 955-968, 2002.

[11] J. M. Sun, W. J. Yi, H. Chen, F. Peng, Y. Zhou, and W. X. Zhang, "Dynamic Responses of RC Columns under Axial Load and Lateral Impact," Journal of Structural Engineering, vol. 149, no. 1, article no. 04022210, pp. 1-18, 2023.

[12] J. M. Sun, H. Chen, F. Yi, Y. B. Ding, Y. Zhou, Q. F. He, et al., "Experimental and Numerical Study on Influence of Impact Mass and Velocity on Failure Mode of RC Columns under Lateral Impact," Engineering Structures, vol. 314, article 118416, 2024.

[13] A. Abay and T. Wondimu, "Numerical Investigation of Bundled RC Column under Impact Load," Advances in Civil Engineering, vol. 2021, no. 1, article no. 5587576, 2021.

[14] Y. Fu, X. Yu, X. Dong, F. Zhou, J. Ning, P. Li, et al., "Investigating the Failure Behaviors of RC Beams without Stirrups under Impact Loading," International Journal of Impact Engineering, vol. 137, article no. 103432, pp. 1-11, 2020.

[15] B. Liu, W. Fan, W. Guo, B. Chen, and R. Liu, "Experimental Investigation and Improved FE Modeling of Axially-Loaded Circular RC Columns under Lateral Impact Loading," Engineering Structures, vol. 152, pp. 619-642, 2017.

[16] H. M. I. Thilakarathna, D. P. Thambiratnam, M. Dhanasekar, and N. Perera, "Numerical Simulation of Axially Loaded Concrete Columns under Transverse Impact and Vulnerability Assessment," International Journal of Impact Engineering, vol. 37, no. 11, pp. 1100-1112, 2010.

[17] Y. Song, J. Wang, and Q. Han, "Dynamic Performance of Flexure-Failure-Type Rectangular RC Columns under Low-Velocity Lateral Impact," International Journal of Impact Engineering, vol. 175, article no. 104541, pp. 1-20, 2023.

[18] J. Zhong, C. Song, J. Xu, Y. Cheng, and F. Liu, "Experimental and Numerical Simulation Study on Failure Mode Transformation Law of Reinforced Concrete Beam under Impact Load," International Journal of Impact Engineering, vol. 179, article no. 104645, pp. 1-22, 2023.

[19] Y. Liu, A. Dong, S. Zhao, Y. Zeng, and Z. Wang, "The Effect of CFRP-Shear Strengthening on Existing Circular RC Columns under Impact Loads," Construction and Building Materials, vol. 302, article no. 124185, pp.1-15, 2021.

[20] W. Fan, X. Xu, Z. Zhang, and X. Shao, "Performance and Sensitivity Analysis of UHPFRC-Strengthened Bridge Columns Subjected to Vehicle Collisions," Engineering Structures, vol. 173, pp. 251-268, 2018.

[21] H. Sharma, S. Hurlebaus, and P. Gardoni, "Performance-Based Response Evaluation of Reinforced Concrete Columns Subject to Vehicle Impact," International Journal of Impact Engineering, vol. 43, pp. 52–62, 2012.

[22] S. Auyeung, A. Alipour, and D. Saini, "Performance-Based Design of Bridge Piers under Vehicle Collision," Engineering Structures, vol. 191, pp. 752–765, 2019.

[23] R. Cao, S. El-Tawil, A. K. Agrawal, X. Xu, and W. Wong, "Behavior and Design of Bridge Piers Subjected to Heavy Truck Collision," Journal of Bridge Engineering, vol. 24, no. 7, article no. 04019057, 2019.

[24] D. B. Zhao, W. J. Yi, and S. K. Kunnath, "Shear Mechanisms in Reinforced Concrete Beams under Impact Loading," Journal of Structural Engineering, vol. 143, no. 9, article no. 04017089, 2017.

[25] D. B. Zhao, W. J. Yi, and S. K. Kunnath, "Numerical Simulation and Shear Resistance of Reinforced Concrete Beams under Impact," Engineering Structures, vol. 166, pp. 387-401, 2018.

[26] G. Gholipour, C. Zhang, and A. A. Mousavi, “Effects of Axial Load on Nonlinear Response of RC Columns Subjected to Lateral Impact Load: Ship-Pier Collision,” Engineering Failure Analysis, vol. 91, pp. 397-418, 2018.

[27] W. Zhao, J. Ye, and J. Qian, “Dynamic Behavior and Damage Mechanisms of Reinforced Concrete Piers Subjected to Truck Impact,” Engineering Failure Analysis, vol. 121, article no. 105158, pp. 1-21, 2021.